A pressure-coupled Representative Interactive Linear Eddy Model (RILEM) for engine simulations

Downloaded from: https://research.chalmers.se, 2025-12-05 04:39 UTC

Citation for the original published paper (version of record):
Doubiani, N., Kerstein, A., Oevermann, M. (2024). A pressure-coupled Representative Interactive Linear Eddy Model (RILEM) for engine simulations. Fuel, 355.
http://dx.doi.org/10.1016/j.fuel.2023.129423

N.B. When citing this work, cite the original published paper.

research.chalmers.se offers the possibility of retrieving research publications produced at Chalmers University of Technology. It covers all kind of research output: articles, dissertations, conference papers, reports etc. since 2004. research.chalmers.se is administrated and maintained by Chalmers Library

(article starts on next page)

Fuel 355 (2024) 129423

Contents lists available at ScienceDirect

Fuel

journal homepage: www.elsevier.com/locate/fuel

Full length article

A pressure-coupled Representative Interactive Linear Eddy Model (RILEM) for engine simulations

Nidal Doubiani [a,*], Alan R. Kerstein [b], Michael Oevermann [a,c]

[a] Chalmers University of Technology, Gothenburg, Sweden
[b] 72 Lomitas Road, Danville, CA, USA
[c] Brandenburgische Technische Universität Cottbus-Senftenberg (BTU), Germany

ARTICLE INFO

Keywords:
Linear Eddy Model
Turbulence-chemistry interaction
Presumed PDF approach
Pollutant formation
Pressure coupling
Engine combustion

ABSTRACT

The Representative Linear Eddy Model (RILEM) was introduced by Lackmann et al. (2018) as an alternative modeling approach to simulate turbulent non-premixed combustion in engines. The model utilizes a RANS approach for turbulence and the Linear Eddy Model (LEM) with a presumed probability density function (PDF) approach for combustion closure. A distinct feature of RILEM is its potential to handle arbitrary combustion regimes and the consideration of complex physical phenomena such as differential diffusion effects. The original version of RILEM implemented a volume-based coupling between LEM and the flow solver. This work presents a new variant of RILEM, i.e., Multiple Representative Interactive Linear Eddy Model (MRILEM) based on a pressure-based coupling, to overcome some deficiencies of the original RILEM, namely statistical fidelity. Due to the introduced pressure coupling, the effects of heat losses (wall heat fluxes, latent heat of evaporation) on combustion are intrinsically included via the pressure trace. Furthermore, we introduce a new step function PDF for the progress variable defined by its mean value only. Issues with an incomplete solution space for mixture fraction and progress variable due to the stochastic nature of LEM are remedied with a PDF scaling technique, aided by a novel parameterization of the progress-variable PDF The new variant of RILEM is evaluated using part- and full-load cases of a heavy-duty metal engine. The impact of utilizing multiple LEM lines on the completeness of the solution space and its influence on the distribution of scalar values in the CFD domain was demonstrated. Results for pressure trace, flame structure, and CO emissions are analyzed and compared with simulations using the Multi-Zone Well-Mixed Model (MZWM) model and experiments. While pressure traces agree well among the different models and experiments, noteworthy differences are observed between the models regarding CO emissions and temperature. Effects of turbulence chemistry interaction were noticed when comparing MRILEM to the results of the MZWM simulation, namely flame brush and species mass fraction distribution.

1. Introduction

The undeniable impact of human-made carbon dioxide emissions on climate change urges humanity to reduce the usage of fossil fuel combustion. An essential role in this effort plays the transport sector which is responsible for roughly one-fifth [1] of the worldwide CO_2 emissions. Many countries have defined and committed themselves to roadmaps implementing severe reductions in CO_2 emissions in the transport sector over the following decades, as well as continuously tightening emissions legislations to reduce the harmful impact of combustion-related emissions on human health, such as particulate emissions. Even with the rapid progress in electrically motored vehicles, the internal combustion engine will likely be relevant for some decades, particularly for long-range of heavy-duty trucks and ships. Therefore, there is a strong need to further improve internal combustion engines in terms of efficiency and emissions. Refined physical models and numerical simulations have become indispensable tools, both in academia and industry, to understand and improve the physical details of combustion and to develop and improve engines. However, new combustion concepts, e.g., dual fuel combustion or partially-premixed combustion ignition (PPCI), and utilization of alternative fuels such as hydrogen or synthetic fuels require the adaptation and improvement of existing combustion models or the development of new models in order to provide predictive simulation tools for research and development.

Several turbulent combustion models have been developed, often limited to either premixed or non-premixed combustion as utilized in spark ignition or diesel engines, respectively. Flamelet models [2],

* Corresponding author.
E-mail address: nidal@chalmers.se (N. Doubiani).

https://doi.org/10.1016/j.fuel.2023.129423
Received 18 April 2023; Received in revised form 19 July 2023; Accepted 4 August 2023
Available online 16 August 2023
0016-2361/© 2023 The Author(s). Published by Elsevier Ltd. This is an open access article under the CC BY-NC-ND license (http://creativecommons.org/licenses/by-nc-nd/4.0/).

initially introduced for non-premixed cases, assume the formation of laminar flame structures in a turbulent field. In non-premixed combustion, flamelet models are based on the scalar dissipation rate concept [3], which describes the diffusive process of a reactive scalar in the mixture fraction space. In premixed combustion, flamelet models utilize the combustion progress variable or level set approaches [4,5]. The parametric coupling that flamelet models are based on can cause over- and under-estimations of the combustion process because of the indirect representation of turbulence via scalar dissipation rate [6]. Few combustion models can be regarded as universally valid and applicable, in principle, for all combustion modes and regimes. Among them are transported PDF (T-PDF) [7] models and models utilizing the linear eddy model (LEM) as a combustion model.

T-PDF models are primarily based on advancing a transport equation for the joint PDF of scalars. T-PDF is a regime- and mode-independent combustion model that accounts for turbulence chemistry interactions (TCI) via micro-mixing models. While chemistry and advection are treated precisely in T-PDF models, molecular mixing needs to be modeled with so-called micro-mixing models, e.g., Interaction by Exchange with the Mean (IEM) or the Coalescence dispersion (C-D) [8–10]. Other models used for both premixed and non-premixed combustion are the Well or Perfectly-stirred reactor (PSR) models and variants such as partially stirred reactor (PaSR) models. While no turbulence chemistry interaction is taken into account in PSR models [11], it is considered in PaSR by the introduction of a mixing time scale [12,13]. These models are popular in the engine community and are used for comparison in this work.

The linear Eddy Model was introduced as a scalar mixing model for non-reactive flows [14–16], and was later extended to treat turbulent reactive flows [17,18]. It was used to simulate combustion as a stand-alone model [19] and as a sub-grid scale model for large-eddy simulation (LES) [20,21]. LEM resolves all spatial and temporal scales on a one-dimensional domain (analogous to a direct numerical simulation (DNS) in terms of resolution), making it a candidate for a proper mode- and regime-independent turbulent combustion model. The modeling aspect of LEM lies in the reduced spatial dimensionality and how turbulence is represented on the one-dimensional line via stochastic re-arrangement events called triplet maps. Highly unsteady effects such as extinction and re-ignition events are captured by LEM without supplementary modeling.

In LES-LEM [22], an LEM is solved in each large-eddy simulation (LES) computational cell. Resolved large-scale advection is implemented by moving parts of LEM domains between neighboring LES cells in a Lagrangian way [23]. LES-LEM has been successfully used to describe turbulent combustion under different flow conditions for non-premixed [20], and premixed combustion [24,25]. The main drawback of LES-LEM is its computational cost making it unattractive for industrial use and implementation in commercial software packages.

A computationally less demanding model than LES-LEM for engine combustion simulations has recently been presented by Lackmann et al. [26]. The so-called Representative Linear Eddy Model (RILEM) carries over some of the main advantages of LES-LEM, namely mode- and regime independence, at a much lower computational cost. RILEM achieves this by utilizing the LEM in a representative way, i.e., instead of solving a LEM in each computational cell as in LES-LEM, only one or a few LEM lines, each representing the complete combustion chamber, are solved and coupled to a flow simulation solving the Reynolds-Averaged Navier–Stokes equations for turbulent flow. RILEM was partly inspired by the Representative Interactive Flamelet (RIF) model [27–29] and utilizes a similar coupling approach between the combustion model (LEM in RILEM, laminar flamelets in RIF) and the flow solver via a presumed PDF approach with mixture fraction and progress variable as the independent variables of the PDF. Although the models feature some similarities, advancing RILEM differs fundamentally from RIF; instead of advancing laminar combustion directly in mixture fraction space or a canonical flow situation (e.g., a counterflow) and only a parametric allowance of turbulence-chemistry interaction via, e.g., the scalar dissipation rate, each LEM in RILEM advances a one-dimensional physical domain with a statistical representation of the complete combustion chamber covering all physics such as turbulence, chemistry, and fuel injection. The (unsteady) driving parameters for the LEM models, such as characteristic values of turbulence kinetic energy, turbulent length scales, and fuel injection rates, are communicated in each time step from the flow solver to each LEM.

Table 1 summarizes development steps on RILEM including this work. In previous implementations of RILEM [26,30,31], the coupling between the flow solver and the LEM line was realized by a volume constraint, i.e., the volumes of the flow solver domain and the LEM domain always match while the pressure is allowed to deviate. As a result of this coupling, heat losses such as wall heat losses and latent heat of evaporation required additional modeling on the LEM line. However, these are usually modeled in detail on the CFD side. In [26,30], RILEM was tested on the Sandia spray B case for three different initial in-cylinder temperatures in [30] and one temperature in [26] but with a more detailed focus on fundamental aspects of the approach. The LEM solutions were conditioned to mixture fraction only, and the thermochemical state was predicted using the conditioned LEM solutions and a presumed β-PDF approach. Despite issues with a realistic representation of highly unsteady combustion phenomena, the results presented in that paper provided a sound proof of concept and demonstrated the potential of RILEM to realistically predict engine combustion. For a more realistic representation of highly unsteady combustion phenomena, an improved variant of RILEM was presented in [31], where a reaction progress variable was added as an additional independent variable. Integration in mixture fraction space was based on the presumed β-PDF, whereas a Dirac δ-peak was chosen for the reaction progress variable. Coupling between the CFD domain and LEM was achieved via volume coupling using a single LEM line. The approach was successfully evaluated on a heavy-duty Volvo diesel engine with a compression ratio of 15.8:1. Ignition delay as well as heat release rates were reasonably well predicted compared to experimental data and against simulation results obtained with an MZWR model.

Further investigations with RILEM on different engine cases revealed certain shortcomings of the volume-coupled RILEM [26,30,31] approach.

In this paper, we discuss further improvements of RILEM to address and overcome those shortcomings: First, to better utilize the detailed modeling of heat losses within the CFD flow solver on the LEM side, we introduce a pressure-based coupling for RILEM. The pressure coupling was implemented and tested for a Spherical Stand-Alone Linear Eddy Model (SSALEM) in [32], where the driving parameters were extracted from a MZWM reacting case. SSALEM can be considered a model among simpler models such as zone models [33] for CFD combustion simulations. Second, to improve the statistical fidelity of the LEM results, we utilize multiple LEMs in parallel within a single RILEM simulation. Third, a novel step-PDF for the progress variable replaces the Dirac δ-peak used in [31] for an improved handling of an incomplete LEM solution space in mixture-fraction-progress-variable space.

The new RILEM variant (MRILEM) is investigated and applied to simulate non-premixed engine combustion in a VOLVO heavy-duty engine under part-load and full-load conditions. The impact of using multiple LEMs on the completeness of the solution space (mixture fraction and progress variable space) is investigated. Simulation results are compared with the MZWM model and experimental data. The results show that MRILEM can successfully capture temperature, major and radical species with combustion closure provided exclusively from a single solution table constructed from multiple LEM realizations. Comparing pressure traces and heat release rates extracted from the three models (MRILEM-PC, RILEM-VC, and MZWM) yielded reasonable agreement both between the different models as well as with experiments. Some differences were noticed when comparing the CFD results from MRILEM and MZWM, the discrepancies include the flame thickness, species distribution, and the ignition process. These results are attributed to the turbulence chemistry interaction that the MRILEM retains, contrary to the MZWM, which neglects it completely.

Table 1
Summary of the development conducted on the RILEM model.

References	[30]	[26]	[31]	[.]
Application cases	Sandia spray B	Sandia spray B	Volvo heavy duty	Volvo heavy duty
Conditioning spaces	Z [200 bins]	Z [200 bins]	Z [200 bins] c [10 bins]	Z [200 bins] c [100 bins]
Coupling scheme	Volume	Volume	Volume	Pressure
Probability density functions	β-Z	β-Z	β-Z Dirac δ-c	β-Z Step-c
Number of LEM lines	1	1	1	16 parallel

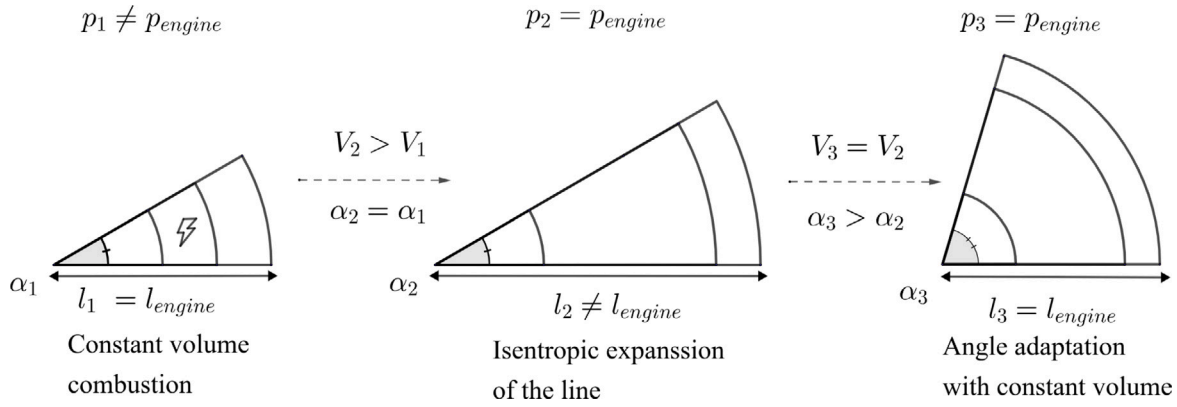

Fig. 1. Split operator strategy and volume correction.

2. Mathematical models

2.1. The Linear Eddy Model

LEM in general and its use in the RILEM context has been described in detail in previous publications [26]. Therefore, we provide only a summary here. LEM describes turbulent reacting flows in two concurrent processes: The first represents the effects of dilation-induced advection, molecular diffusion, and chemical reactions. It involves the time-advancement of the zero-Mach number equations on a one-dimensional domain, enabling the resolution of all relevant spatial and temporal scales. In order to represent volumetric effects on a one-dimensional line consistently (e.g., the time-evolution of the global equivalence ratio during fuel injection), we utilize a spherical formulation of LEM in RILEM, see [26] for details. The spherical formulation allows a consistent representation of the combustion process in the cylinder of an engine on a one-dimensional domain. The second process, turbulent advection, is implemented as a sequence of statistically independent re-arrangement or mapping events governed by a Poisson process in time, each mimicking the impact of turbulent eddies on a one-dimensional scalar profile. The LEM transport equations are given as follows:

$$\rho \frac{\mathrm{d}Y_s}{\mathrm{d}t} = -\frac{1}{r^2}\frac{\mathrm{d}}{\mathrm{d}r}\left(r^2 j_s\right) + M_s \dot{w}_s + \rho \dot{Y}_{s,ev}, \tag{1}$$

$$\rho \frac{\mathrm{d}h}{\mathrm{d}t} = -\frac{1}{r^2}\frac{\mathrm{d}}{\mathrm{d}r}\left(r^2\left[q + \sum_s j_s h_s\right]\right) + \frac{\mathrm{d}p}{\mathrm{d}t} + \rho \dot{h}_{ev}, \tag{2}$$

where ρ denotes density, Y_s mass fraction of species s, M_s the molecular weight, $\dot{w}_s$ the source term due to chemical reactions and $\dot{Y}_{s,ev}$ the source term due to fuel evaporation. h represents enthalpy, q the heat flux, h_s the enthalpy of species s that includes the heat due to formation, p the pressure, and $\dot{h}_{ev}$ the enthalpy contribution due to the added evaporated fuel.

The eddies in LEM are sampled from a prescribed size distribution under the assumption of a Kolmogorov inertial-range scaling [15]:

$$f(l) = \frac{5}{3}\frac{l^{-8/3}}{\eta^{-5/3} - l_t^{-5/3}}, \tag{3}$$

where η is the Kolmogorov length scale and l_t the integral length scale. With the turbulent Reynolds number

$$Re_t = \frac{u' l_t}{\nu}, \tag{4}$$

where ν and u' denote the kinematic viscosity and the root-mean square turbulent velocity fluctuation, respectively, the eddy frequency per unit length is determined via [15]

$$\lambda = \frac{54}{5}\frac{\nu Re_t}{C_\lambda l_t^3}\frac{(l_t/\eta)^{5/3} - 1}{1 - (\eta/l_t)^{4/3}}. \tag{5}$$

with model constant $C_\lambda = 15$ [34]. The Kolmogorov scale η is determined from the inertial-range scaling law $\eta = N_\eta l_t Re_t^{-3/4}$ with model constant $N_\eta = 10.76$ taken from [34]. The location of an eddy event is randomly sampled with a uniform distribution over the LEM domain. The eddy time is sampled under the assumption of a Poisson process with mean occurrence time increment $\Delta\tau_{eddy} = (\lambda L)^{-1}$, where L is the domain size.

From Eqs. (3)–(5) it follows that the driving parameters of the linear eddy model are Re_t and l_t. For stand-alone simulations (SSALEM), these parameters need to be provided as inputs to the simulation; in RILEM, they are calculated from the CFD flow solver and passed after each CFD time step to the LEM, see below. In addition to turbulent eddy events according to the description above, additional eddy events with a fixed eddy size are implemented to model large-scale motion, such as tumble or swirl on the one-dimensional line. For details, we refer to [26].

In typical engine simulations, the length L of the LEM domain is assumed to equal the cylinder bore. This corresponds to a picture of the LEM line being oriented towards the spray axis. However, different engine conditions might require an adjustment of the LEM domain length.

The LEM governing equations are discretized with a second-order scheme in space and time where the stiff chemical source term is integrated using Sundials solver CVODE [35].

2.2. Pressure coupling of spherical Linear Eddy Model

An essential characteristic of how LEM is used in RILEM is that each line represents the complete engine/combustion chamber, not

just a canonical flame or flow configuration (e.g., a shear layer). That implies that all relevant physical processes, such as fuel injection and piston movement, must be modeled on the one-dimensional line. It also offers the possibility to utilize LEM as a computationally affordable stand-alone model to perform engine simulations with a realistic representation of all relevant physical processes as described in [32]. An important consequence of the representative character of the LEM line is the need for a volumetric formulation of the LEM, which is realized via a (double) solid cone geometry of the LEM domain with the assumption of spherical symmetry. For details, we refer to [30]. In this situation, the LEM was coupled to the CFD by prescribing the pressure to avoid modeling the heat loss effects on the line. The length of the LEM line in the current implementation needs to be prescribed. In this work, we set the LEM domain length to a fixed (in time) characteristic length of the engine, e.g., the complete engine bore or a fraction. In order to match the LEM line pressure, which is assumed to be spatially constant, with the prescribed pressure value after each time step of the simulation, we adopt the following *split operator strategy*, see Fig. 1 for illustration:

1. Advance LEM line for time increment Δt under constant volume condition ⇒ local heat release due to combustion and temperature change due to mixing with (cold) fuel lead to a change in pressure of individual LEM cells while length and volumes are kept constant.
2. Isentropic expansion/compression of all cells to the prescribed target pressure at constant cone angle ⇒ length and volume of the LEM domain will change.
3. Adjustment of the cone angle under constant volume conditions to match the prescribed characteristic length of the LEM domain.

It should be noticed that steps 2 and 3 require an adjustment of cell face boundaries on the LEM line.

2.3. RILEM

This article introduces an improved RILEM variant, with a summary of the key features of this model. RILEM, as discussed in [26,31], can predict turbulent non-premixed combustion in engines with reasonable accuracy. The approach utilizes the LEM model as a combustion model in a representative way; see Section 1. The coupling between LEM and CFD flow solver with a presumed PDF approach is reminiscent of laminar flamelet models for turbulent non-premixed combustion. Fig. 2 shows a sketch of the overall coupling approach and will be discussed briefly here.

The CFD solver advances the governing equations of a RANS turbulence modeling approach, i.e., balance equations for global mass, momentum, and energy. Turbulence is modeled using the standard $k-\epsilon$ turbulence model with a modified value $C_{\epsilon 1} = 1.5$ as suggested for an n-dodecane spray flame by the engine combustion network (ECN) [36].

To capture highly unsteady phenomena, the extended RILEM approach [31] introduced a presumed Favre joint-PDF for mixture fraction and reaction progress variable with the assumption of statistical independence [37], i.e.

$$\tilde{P}_{Z,c}(Z,c) = \tilde{P}_Z(Z)\,\tilde{P}_c(c). \tag{6}$$

Knowing the joint PDF of mixture fraction and progress variable, the Favre mean value of any scalar $\phi(Z,c)$ can be evaluated by simple integration:

$$\begin{aligned}\tilde{\phi} &= \int_0^1\int_0^1 \phi(Z,c)\,\tilde{P}_{Z,c}(Z,c)\,\mathrm{d}Z\,\mathrm{d}c \\ &= \int_0^1\int_0^1 \phi(Z,c)\,\tilde{P}_Z(Z)\,\tilde{P}_c(c)\,\mathrm{d}Z\,\mathrm{d}c\end{aligned} \tag{7}$$

In order to evaluate the PDF integral above, we need scalar values ϕ as a function of Z and c. The LEM provides us with a solution in physical space. However, since each cell of the LEM domain hosts a complete thermo-chemical state, we can compute mixture fractions and progress variables in each cell of the LEM domain. Let r be the spatial coordinate of the one-dimensional LEM line and r_i the centroid of LEM cell i. With the discrete LEM solution values $Z(r_i)$, $c(r_i)$ and $\phi(r_i)$, we can define the mapping from physical LEM space to (Z,c) space:

$$Z(r_i),\ c(r_i), \phi(r_i) \longmapsto \phi(Z(r_i), c(r_i)). \tag{8}$$

As given values of Z and c can appear at multiple locations on the LEM line, it is important to note that (8), in general, leads to a multi-valued map. In the case of a multi-valued map, we define the unique value $\phi(Z,c)$ by arithmetic averaging; see below for details. The multi-valued LEM solution in (Z,c) space embodies the intrinsic representation of scalar dissipation rate fluctuations in LEM, i.e., no modeling of those fluctuations is necessary for LEM, whereas it is (in principle) necessary in flamelet models.

The transport equations of $\tilde{Z}$ and $\widetilde{Z''^2}$ are advanced on the CFD:

$$\frac{\partial \bar{\rho}\tilde{Z}}{\partial t} + \frac{\partial \bar{\rho}\tilde{u}\tilde{Z}}{\partial x_j} = \frac{\partial}{\partial x_j}\left[\frac{\mu_t}{Sc_t}\frac{\partial \tilde{Z}}{\partial x_j}\right] + \dot{m}_{ev}, \tag{9}$$

$$\begin{aligned}\frac{\partial \bar{\rho}\widetilde{Z''^2}}{\partial t} + \frac{\partial \bar{\rho}\tilde{u}\widetilde{Z''^2}}{\partial x_j} = \frac{\partial}{\partial x_j}\left[\frac{\mu_t}{Sc_t}\frac{\partial \widetilde{Z''^2}}{\partial x_j}\right] + \\ \frac{2\mu_t}{Sc_t}\frac{\partial \tilde{Z}}{\partial x_j}\frac{\partial \tilde{Z}}{\partial x_j} - \bar{\rho}\tilde{\chi},\end{aligned} \tag{10}$$

where $\dot{m}_{ev}$, μ_t, and Sc_t denote the source term due to evaporation, the turbulent viscosity, and the turbulent Schmidt number, respectively, and μ_t was taken as 0.7. The molecular diffusivity was neglected compared to turbulent diffusivity. In addition, $\tilde{\chi}$ represents the Favre-averaged mean scalar dissipation rate, which is modeled as the following based on [27]

$$\tilde{\chi} = C_\chi \frac{\tilde{\epsilon}}{\tilde{k}}\widetilde{Z''^2} \tag{11}$$

with model constant $C_\chi = 2.0$

We assume the commonly used β-PDF for the mixture fraction Favre PDF $\tilde{P}_Z(Z)$ in (6):

$$P_Z(Z;\tilde{Z},\widetilde{Z''^2}) = \frac{\Gamma(\alpha+\beta)}{\Gamma(\alpha)\Gamma(\beta)} Z^{(\alpha-1)}(1-Z)^{(\beta-1)}, \tag{12}$$

where Γ is the gamma function and α and β are functions of $\tilde{Z}$ and $\widetilde{Z''^2}$. The advancement of the two transport equations gives a value of $\tilde{Z}$ and $\widetilde{Z''^2}$ in each CFD cell, which provides uniquely defined shapes of the presumed PDF in each cell of the CFD domain. In [31], a Dirac δ-peak is assumed as the functional shape of the progress variable PDF. However, using only a few LEM lines in RILEM, it cannot be guaranteed that at each point in time, the complete progress variable space will be filled from the current LEM state. This problem can deteriorate the integrity of the PDF integration in progress variable space; see the discussion below. The progress variable on the LEM is defined as

$$c = \frac{\psi - \psi_u}{\psi_b - \psi_u}, \tag{13}$$

where ψ, ψ_u and ψ_b represent the actual, the unburnt, and burnt scalar quantity, respectively. For a local definition of the progress variable PDF in each CFD cell, an additional transport equation for the Favre mean value of the progress variable $\tilde{c}$ is solved on the CFD side:

$$\frac{\partial \bar{\rho}\tilde{c}}{\partial t} + \frac{\partial \bar{\rho}\tilde{u}\tilde{c}}{\partial x_j} = \frac{\partial}{\partial x_j}\left[\frac{\mu_t}{Sc_t}\frac{\partial \tilde{c}}{\partial x_j}\right] + \bar{\rho}\tilde{\dot{c}}, \tag{14}$$

where $\tilde{\dot{c}}$ denotes the source term of the progress variable transport equation. The evaluation of the source term is crucial for an accurate prediction of unsteady phenomena in turbulent combustion, and there are several options to calculate it. In this work, the Favre mean source term $\tilde{\dot{c}}$ is evaluated similarly to other scalars from the LEM solution. First, we calculate progress variable source term on the LEM, and then condition it on Z and c according to the map (8) as:

$$\dot{c}(Z,c) = \frac{1}{\psi_b - \psi_u}\frac{\mathrm{d}\psi}{\mathrm{d}t}, \tag{15}$$

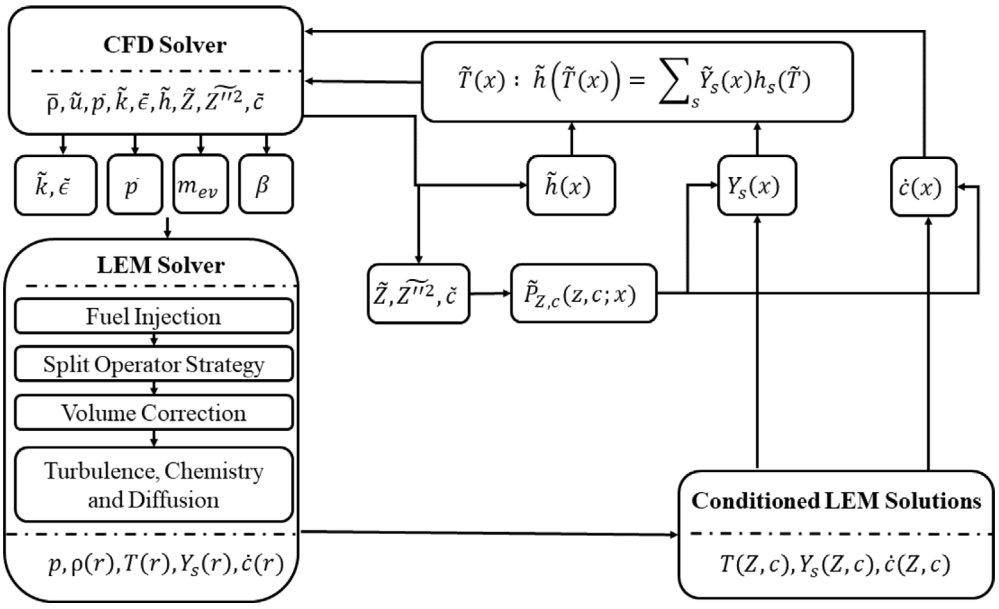

Fig. 2. RILEM code framework.

where $\mathrm{d}\psi/\mathrm{d}t$ is the consumption/production rate of the scalar ψ. The Favre mean $\tilde{c}$ is calculated in a second step by integration with the PDF as in (7).

Compared to the assumed β-PDF for the distribution of the mixture fraction – which is very well established (particularly in flamelet models for turbulent non-premixed combustion) – the prescription of the shape of the PDF for the reaction progress variable is more debatable. Due to its simplicity, the Dirac delta function is a prevalent assumption. The Dirac delta PDF often produces reasonable results. An additional reason for its popularity is that it is sufficient to solve an equation for the mean value of the reaction progress variable, $\tilde{c}$. More complex PDFs such as the β-PDF require models or an additional transport equation for the variance of the reaction progress variable $\widetilde{c''^2}$.

Due to the conceptual approach of RILEM, where each LEM line represents the complete combustion chamber, we encounter the situation that the mixture fraction-progress variable space usually is not entirely represented by the instantaneous solution on the LEM line(s) in the simulation, see detailed discussion below. Therefore, the assumption of a Dirac delta PDF for the progress variable needs to be revised, as it can lead to situations where no solution is available at or close to the local value of the progress variable. For RILEM, it is, therefore, preferable to assume a PDF of c with support on the complete range of possible values, i.e., $\tilde{P}_c(c) > 0$ for all $c \in [0, 1]$.

Here, we propose a new step-function PDF which is uniquely defined by the Favre mean value $\tilde{c}$ only, i.e., there is no need to solve an additional transport equation for $\widetilde{c''^2}$, in the following way.

$$\tilde{P}_c(c; \tilde{c}) = \begin{cases} \frac{1-\tilde{c}}{\tilde{c}} & 0 \le c < \tilde{c}, \\ \frac{\tilde{c}}{1-\tilde{c}} & \tilde{c} \le c \le 1. \end{cases} \tag{16}$$

For $\tilde{c} = 0.5$, the step-function PDF results in the uniform distribution, and in the limits $\tilde{c} = 0$ and $\tilde{c} = 1$, the step-function PDF degenerates to the physically meaningful Delta-PDF Fig. 3 shows shapes of the step function PDF for different values of $\tilde{c}$. The step-function PDF, in combination with the PDF scaling described below, leads to a computationally robust calculation of mean values according to (7) for RILEM.

The Favre-averaged temperature $\tilde{T}$ can be calculated by PDF integration (7) from the conditioned LEM solution. However, here we use the enthalpy of the CFD solver and the Favre mean values of the species mass fractions to iterate the temperature in each computational cell of

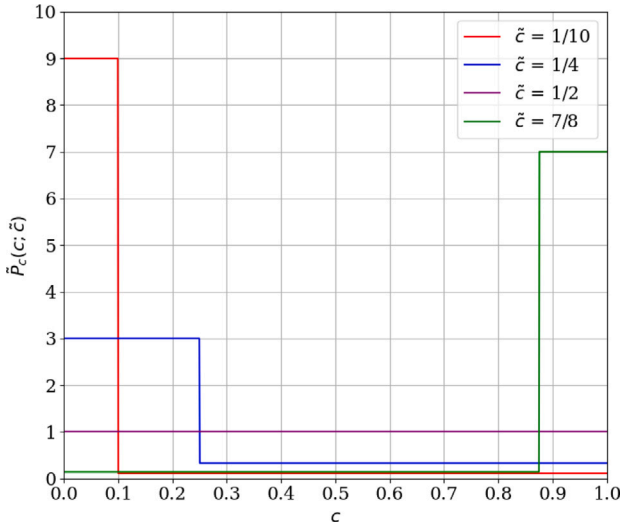

Fig. 3. Step function PDF representation for $\tilde{c}$ = {1/10, 1/4, 1/2, 7/8}.

the CFD domain using the caloric equation of state:

$$\tilde{h}_k(\tilde{T}) = \sum_{s=1}^{N} \tilde{Y}_{s,k} h_s(\tilde{T}), \tag{17}$$

with

$$h_s(T) = \Delta h_s^0 + \int_{T^0}^{T} c_{p,s}(T)\,\mathrm{d}T, \tag{18}$$

where h_s denotes the mass-specific enthalpy value of the species s, Δh_s^0 the standard heat of formation for species s, and $c_{p,s}$ the mass specific heat capacity of species s at constant pressure. Thermo-chemical data, transport coefficients, and reaction rates are calculated using the software package Cantera [38].

Spray injection and evaporation is simulated with an Eulerian–Lagrangian approach implemented in the OpenFOAM ICE library Lib-ICE 2.2.5 developed by Politecnico di Milano [39]. In the Eulerian–Lagrangian approach the continuous gas phase is simulated solving the standard balance equations for mass, momentum and energy/enthalpy

in an Eulerian frame of reference whereas the spray is represented via discrete liquid parcels individually tracked in a Lagrangian way. Grouping droplets with identical properties into representative parcels reduces computational cost. Two way coupling between dispersed droplet phase and gas phase is realized with the particle-source-in-cell approach where detailed models/correlations for drag, heat-up and evaporation provide source terms for momentum, mass and energy in each computational cell containing liquid parcels/droplets. Spray atomization is modeled via the blob approach where parcels are introduced into the domain with a characteristic diameter of the injector nozzle hole followed by secondary breakup modeled using the Huh–Gosman model [40] which features a characteristic length and time scale to calculate the disintegration process of larger droplets into smaller ones. The atomization process terminates once the critical Weber number is reached, where surface tension energy prevents further disintegration. The secondary breakup model was complemented by coupling the Huh–Gosmann model with the Pilch–Erdman correlation [41], which provides the breakup time necessary for the droplet diameter calculation. A Ranz–Marshall correlation [42] is applied to evaluate heat transfer between gas phase and droplet parcels. For details of the spray-model we refer to [43].

2.4. LEM solution table

The LEM in RILEM provides scalar values such as mass fractions conditioned on mixture fraction and progress variable, which are then integrated with a presumed PDF according to (7) to get Favre averaged scalar quantities $\tilde{\phi}$. The implementation of the mapping (8) and the integration (7) are discrete, i.e., both mixture fraction and progress variable spaces are divided into discrete bins. Let n_Z, n_c denote the number of discrete bins and ΔZ_i, Δc_j the sizes of bins i and j in mixture fraction and progress variable space, respectively, with $\sum_{i=1}^{n_Z} \Delta Z_i = \sum_{j=1}^{n_Z} \Delta c_j = 1$. The PDF integral (7) in its discrete form can be written as

$$\tilde{\phi} = \sum_{j=1}^{n_c} \sum_{i=1}^{n_Z} \phi(Z_i, c_j) \tilde{P}_Z(Z_i)\, \tilde{P}_c(c_j)\, \Delta Z_i\, \Delta c_j, \tag{19}$$

where Z_i and c_j are the midpoints of bin i in mixture fraction and bin j in progress variable space defined by $Z_i = \sum_{k=1}^{i-1} \Delta Z_k + \Delta Z_i/2$, $i = 1, \ldots, n_Z$ and $c_j = \sum_{k=1}^{j-1} \Delta c_k + \Delta c_j/2$, $j = 1, \ldots, n_c$. In the following we write ϕ_{ij} short for $\phi(Z_i, c_j)$ and call the full set of ϕ_{ij}, $i = 1, \ldots, n_Z$, $j = 1, \ldots, n_c$ a *solution table*.

To perform the discrete PDF integration (19) values ϕ_{ij} from the LEM must be available for all bins, i.e., a completely filled solution table is required. However, this can, in general, not be guaranteed. This artifact originates from the concept of RILEM, where each LEM line represents the complete combustion chamber with a realistic representation of all physical processes. E.g., prior to fuel injection, no fuel is present on the LEM line; therefore, only values for $Z = 0$ and $c = 0$ exist. The actual values of Z and c, depend on turbulent mixing, diffusion, and chemical reaction progress. It has been noticed in several simulations with RILEM that the fidelity of the solution strongly depends on the available data in the solution table and is very sensitive to the initialization of the table. In the following, we discuss the adopted strategy to handle situations when the solution table is not entirely filled. The strategy comprises three different sub-components, described in the following three subsections.

2.5. PDF scaling

The first approach to handle bins in the solution table containing no data is to ignore them and exclude them from the integration in (19). Let $\mathcal{N}_Z$ and $\mathcal{N}_c$ be the set of indices Z_i and c_j containing data. The double sum in (19) is then replaced by

$$\tilde{\phi} = \sum_{j \in \mathcal{N}_c} \sum_{i \in \mathcal{N}_Z} \phi(Z_i, c_j) \tilde{P}^{\star}_Z(Z_i)\, \tilde{P}^{\star}_c(c_j)\, \Delta Z_i\, \Delta c_j, \tag{20}$$

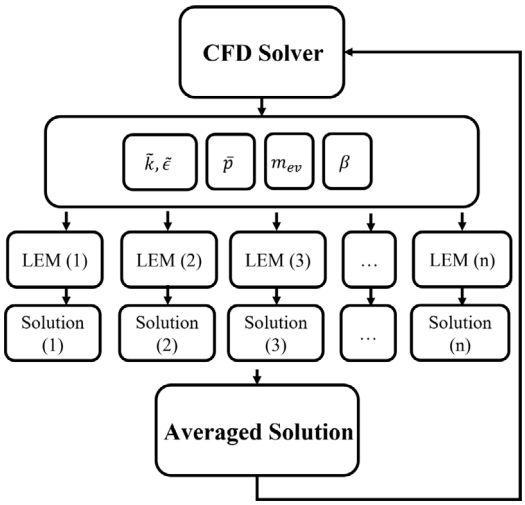

Fig. 4. MRILEM code framework.

where $\tilde{P}^{\star}_{\xi}$, $\xi \in \{Z, c\}$ is a scaled PDF to ensure the normalization condition $\sum_{i \in \mathcal{N}_{\xi}} \tilde{P}^{\star}_{\xi}(\xi_i) \Delta \xi_i = 1$:

$$\tilde{P}^{\star}_{\xi}(\xi_i) = \frac{\tilde{P}_{\xi}(\xi_i)}{\sum_{i \in \mathcal{N}_{\xi}} \tilde{P}_{\xi}(\xi_i) \Delta \xi_i}. \tag{21}$$

Scaling of the PDF is always applied in this work when the solution table is not entirely filled.

2.6. Multiple RILEMs (MRILEM)

Using just a single LEM line in RILEM often leads to a solution table with several unfilled bins. Due to the stochastic nature of LEM, each LEM simulation can be regarded as one realization of a turbulent flow. It is, therefore, natural to increase the statistical fidelity by increasing the number of realizations, i.e., by running multiple LEMs simultaneously in parallel. The LEM lines are all driven with identical parameters from the CFD flow solver. However, each implements a different series of turbulent eddy events (which is easily realized by setting different initial random seeds for each LEM). The MRILEM framework is sketched in Fig. 4.

An essential feature of the pressure-coupled MRILEM is the implicit coupling of all LEM lines due to the CFD pressure. Suppose only one of the lines has reached local conditions for auto-ignition resulting in a positive value for the progress variable source term (15). In that situation, initiation of combustion on the CFD is started by that – and only that – LEM line. This means that this positive value of the progress variable source term will be communicated to and influences the *averaged* LEM solution table. As a result of heat release, pressure on the CFD domain will rise, and the elevated pressure value will be communicated to all LEM lines enhancing the conditions for auto-ignition. It should be noted that the impact of just one ignited LEM line does only weakly promote combustion on the other lines due to the averaging process. All LEM tables, except the average/general LEM table, are consistently cleaned after each time step. This way, they always only carry information of the current time step. This coupling is perfectly consistent with the real combustion physics in an engine which was not present in the previously presented volume coupled RILEM [30,31].

From all LEM lines a single solution table is constructed. To obtain a unique scalar value $\phi_{ij} = \phi(Z_i, c_j)$ for bin (Z_i, c_j) we apply arithmetic averaging:

$$\phi_{ij} = \frac{1}{n_{ij}} \sum_{k \in \mathcal{N}_{ij}} \phi^k_{ij}, \tag{22}$$

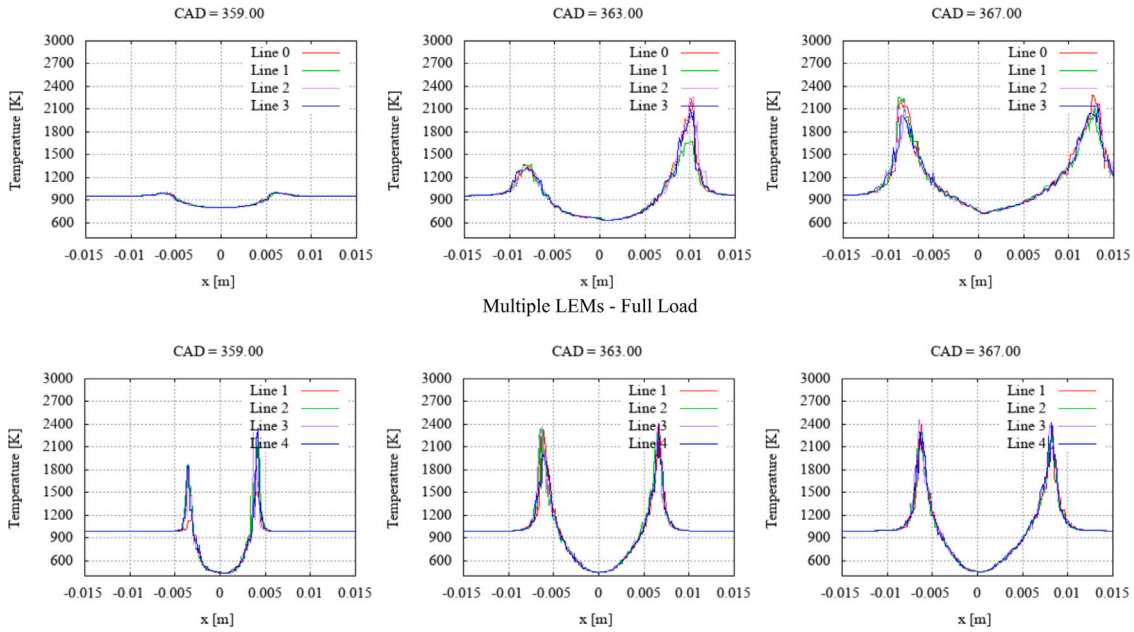

Fig. 5. Representation of temperature field of multiple LEM lines in physical space for CAD = 359.00 (left), 363.00 (center), 367.00 (right) for part-load (above) and full-load (below). (For interpretation of the references to color in this figure legend, the reader is referred to the web version of this article.)

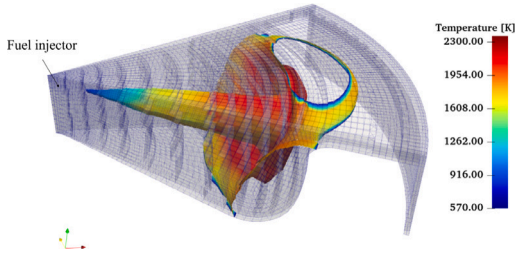

Fig. 6. Representation of the computational domain, location of the injector, and the temperature contour for $Z = 0.04$ part-load case at CAD = 363.00.

Table 2
Experimental setup for both the part-load and full-load cases.

		Part-load	Full-load
Initial pressure (bar)		1.69	4.25
Initial temperature (K)		395	404
Composition (% mass)	O_2	16.5	18.9
	N_2	75.3	75.8
	CO_2	5.97	3.91
	H_2O	2.26	1.48
Injected mass (mg)		13	47
Start of injection		3.1° bTDC	4.7° bTDC
End of injection		3.3° aTDC	16.7° aTDC

where $\mathcal{N}_{ij}$ is the set of LEM grid cells across *all* LEM lines with $Z^k \in [Z_i - \Delta Z_i/2, Z_i + \Delta Z_i/2]$, $c^k \in [c_j - \Delta c_j/2, c_j + \Delta c_j/2]$ and ϕ_{ij}^k is the value of ϕ_{ij} in cell k of the set.

2.7. LEM solution persistence

Preferably at each time step, the general/averaged solution should be based only on the available solutions on the LEM lines at that time step. However, in contrast to, e.g. flamelet models, where the entire mixture fraction space is always completely filled, in LEM this is not guaranteed due to the representation of the combustion process in physical space. Situations with an incomplete solution space in mixture and/or progress variable space can enhance the PDF scaling effect, which may distort the CFD solution. In order to minimize the number of empty bins in the general/averaged solution table, solutions from previous times steps are kept in the general table in case that slot is not present in the current LEM solution. Whenever a solution for a bin in Z, c space is available from at least one LEM line, it will be overwritten by the average of the available LEM data.

2.8. Multi-Zone Well-Mixed Model (MZWM)

MRILEM results are compared to the Multi-Zone Well-Mixed model (MZWM) output to assess its effects on turbulence chemistry interactions. The MZWM model is based on the Well Stirred Reactor (WSR) model, where each CFD cell is treated as a homogeneous reactor. To reduce computational cost compared to the WSR model which solves the full chemistry in each computational cell, in the MZWM model the chemistry is jointly advanced for CFD cells with similar thermochemical states. Multiple zones of similar thermochemical states are defined based on temperature and equivalence ratio. For details we refer to [6,44].

3. Experimental and numerical setup

3.1. Experimental setup

The investigated case is a Volvo 13L six-cylinder Heavy-duty truck engine with a compression ratio of 15.8:1. A part-load and a full-load case are investigated, the details are summarized in Table 2.

3.2. Computational setup

The simulations were conducted using the CFD software OpenFOAM 2.2.x [45] on which MRILEM was implemented. The LEM solver is based on the one-dimensional turbulence framework initially developed by [46]. The CFD computational domain shown in Fig. 6 represents a sector of combustion chamber with a 6-hole injector. It incorporates 31 365 spray-oriented hexahedral cells, generated using POLIMI's in-house automatic mesh generator implemented in Lib-ICE [47]. A reduced n-dodecane mechanism of 54 species and 269 chemical reactions proposed by [48] was employed in this simulation. The scalar ψ is chosen as oxygen mass fraction for progress variable definition.

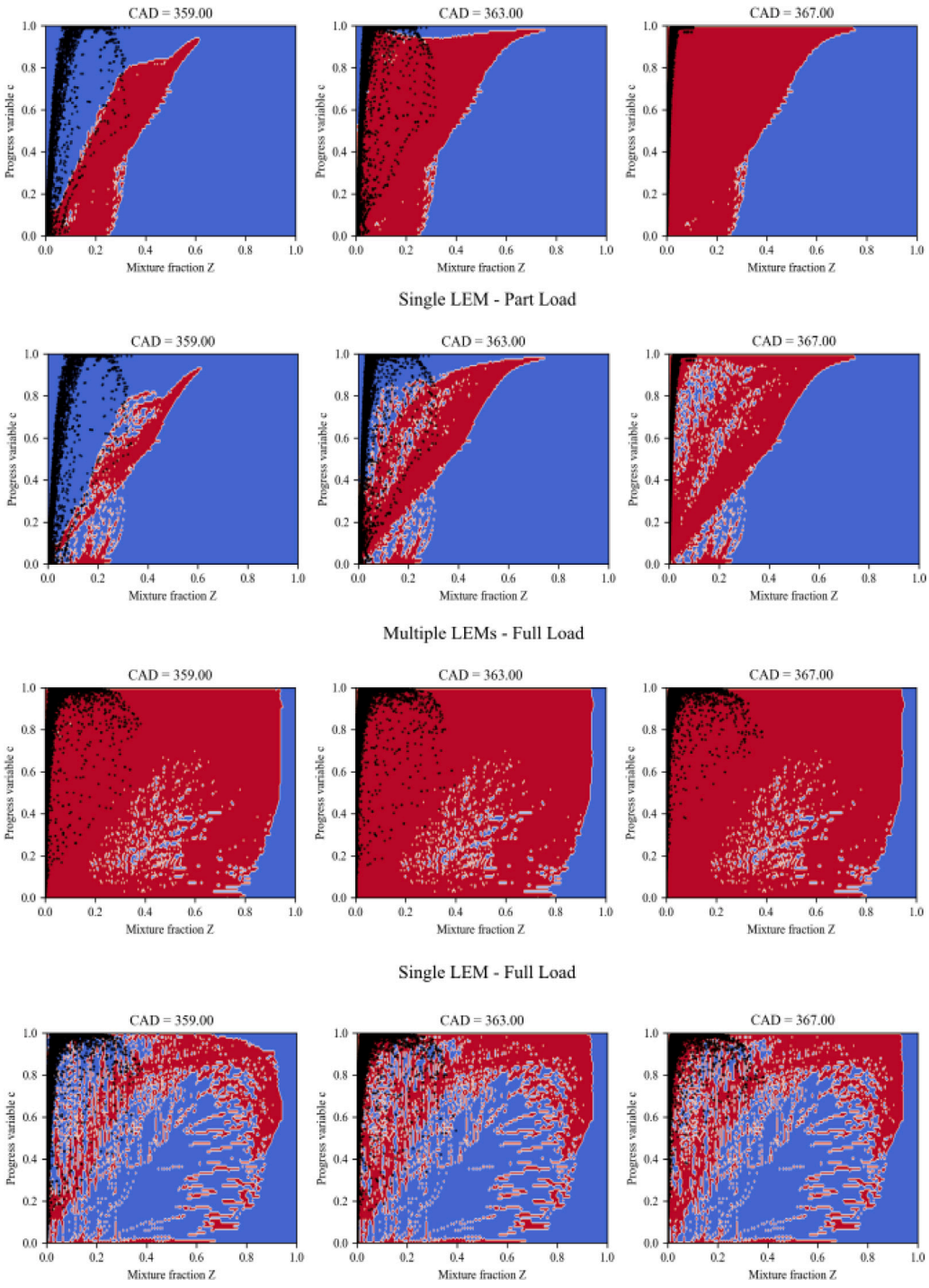

Fig. 7. Representation of the CFD statistics $(\tilde{Z}, \tilde{c})$ represented by black dots, and the LEM uncovered solutions by advancing multiple LEM lines (above) and a single LEM line (below) visualized by the red heatmap in (Z, c)-space, at CAD = 359.00 (left), 363.00 (center), 367.00 (right). (For interpretation of the references to color in this figure legend, the reader is referred to the web version of this article.)

4. Results and discussions

MRILEM was advanced using 16 LEM lines with scaling of mixture fraction and progress variable PDFs. As described above, solution tables are initialized empty to avoid inconsistent thermo-chemical states.

4.1. LEM in physical space

Fig. 5 shows snapshot profiles of temperature on different LEM lines for the part- and full-load cases at different CAD values. The different colors in the figure represent an evolution of different LEM lines depending on the selected turbulent statistics. Both small and large-scale turbulent eddies, which model (large scale) swirl in the combustion chamber, were considered in this simulation.

4.2. LEM solution population

Fig. 7 portrays the population of the (Z, c)-space for part- and full-load case using single and multiple LEMs. Here, blue indicates regions in (Z, c)-space which have not been accessed by any of the LEMs and

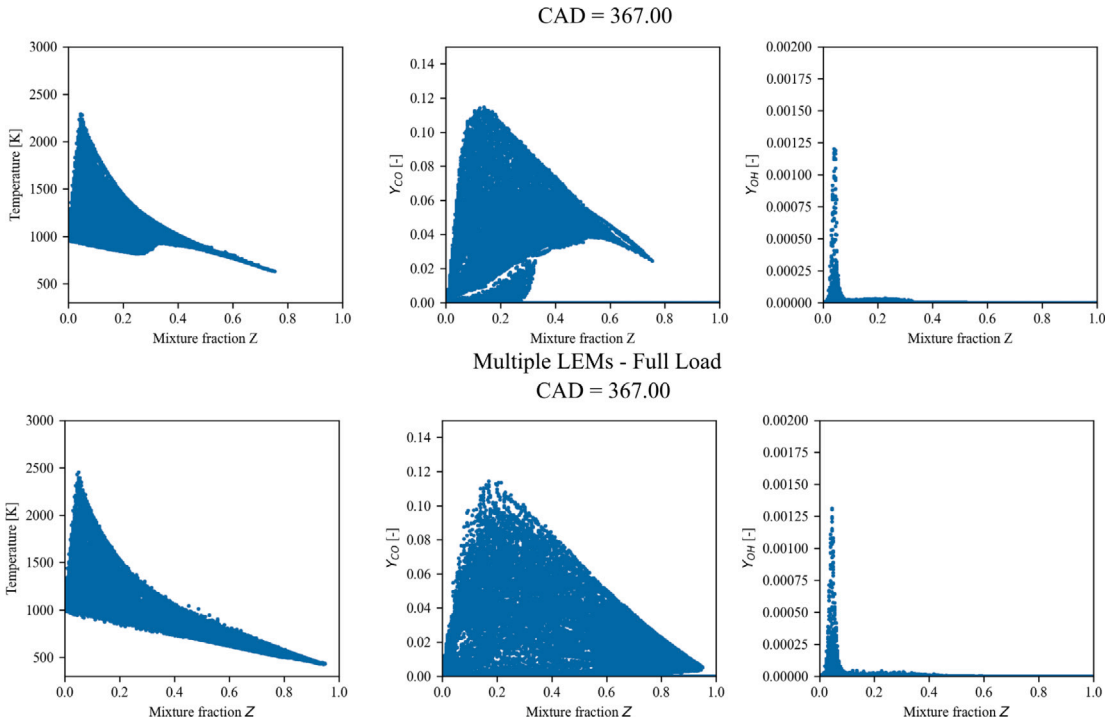

Fig. 8. Scatter plots in mixture fraction space for temperature (left), CO mass fraction (center), and OH mass fraction (right) for part-load (above) and full-load (below) at CAD = 367 obtained with MRILEM.

red indicates regions in (Z, c)-space which have been accessed by at least one LEM. In the same figure, data obtained from the solution of the transport Eqs. (9) and (14) on the CFD domain are depicted by black dots. It is clearly observable, how the space is populated with increasing time or CAD and that running multiple LEMs simultaneously fills the space much quicker and more complete than a single LEM which leave many unfilled spots inside already accessed areas in (Z, c)-space. However, when overlapping the occupied (Z, c) of the CFD side and the LEM solutions, it appears that for the part load case at CAD = 359, both a single LEM line and multiple LEM lines in MRILEM do not provide data the CFD requires in the region $0 \leq Z \leq 0.3$ for $0.15 \leq c \leq 1$. There are a few mechanisms which can cause this issue in principle: First, a mismatch in fuel–air mixing on the CFD and the LEM side. Fuel–air mixing on the LEM side is always delayed by one or a few time steps relative to the CFD solution as liquid fuel evaporation and mixing needs to happen on the CFD domain first before any fuel is seen on the LEM side. Additionally, and likely more relevant, is a mismatch of fuel–air mixing due to large scale 3D effects which can be represented on the LEM domain only by modeling (here, via large eddy events). However, the results shown in Fig. 7 show a mismatch in progress variable space for higher values of c for a given mixture fraction and not for the mixture fraction *per se*. This points to the second reason which can potentially cause a mismatch between CFD and LEM solution space: reaction progress is always determined by reaction progress on the LEM line(s) which drives the CFD progress variable source term in $\tilde{c}$ in Eq. (14) via PDF integration of the LEM source term. This implies that reaction progress on the LEM in principle is always ahead of reaction progress on the CFD side, but the plots in Fig. 7 show actually the opposite at CAD = 359 for the low load case (both single and multiple LEM) and for all CAD values for single LEM and full load. A third reason, which explains the observed mismatch here, is a difference between the shape of the presumed PDF on the CFD side and the implicitly predicted PDF of the LEM model at this early stage in the combustion process for the low load case which will be discussed below.

The situation has relaxed at CAD = 363 and 367 where, when using multiple LEMs, the occupied (Z, c)-space observed on the CFD is almost completely represented by the LEM solutions. For the full load case the (Z, c)-space is occupied much quicker compared to the part load case and MRILEM manages to almost completely cover the (Z, c)-space observed on the CFD side for all CAD values. However, the plots for both part and full load cases proof that running RILEM with just one LEM is not sufficient to represent the (Z, c) solution space encountered on the CFD domain.

It should be noted that the PDF integrals in (7) formally require a completely filled (Z, c)-space which is almost always impossible to achieve. However, from a practical point of view, this is usually not a problem as those areas are usually characterized by vanishing probabilities and therefore do not contributing significantly to the integral. This will be explained in more detail in the next section.

4.3. PDF statistics and LEM solution

Fig. 9 shows shapes of the presumed PDFs for Z and c, i.e. β- and step-PDF, respectively, for three representative shape defining conditions at the same three different CAD values as in Fig. 7. Available LEM temperature solutions found on multiple LEM lines at the given CAD values conditioned an Z and c are represented as dots.

As discussed above, the situation of missing data points in (Z, c)-space is most dominant at CAD = 359 for the low load case. From the plots $\langle T|Z\rangle$ and $\langle T|c\rangle$ for that CAD value in Fig. 9 it can be clearly observed that, e.g., the presumed step-PDFs for $\tilde{c} = 0.5$ and $\tilde{c} = 0.8$ are non-zero for larger values of c where no LEM data is available. For $\tilde{c} = 0.8$ there is actually no overlap at all between values of non-zero PDF and available LEM data. The situation is also visible in the plots $\langle T|Z\rangle$ for CAD = 359 where, e.g., no LEM data for the case $\tilde{Z} = 0.15$, $\tilde{c} = 0.8$ is available in the region around $Z = 0.15$, where the β-PDF has its peak value. The fact that the RILEM approach is still capable to predict quite reasonable ignition histories even under such difficult data conditions demonstrates the robustness and effectiveness of the introduced PDF scaling approach together with the LEM solution persistence.

At later CAD values 363 and 367 for the part load case and all CAD values for the high load case, a more or less full overlap of regions

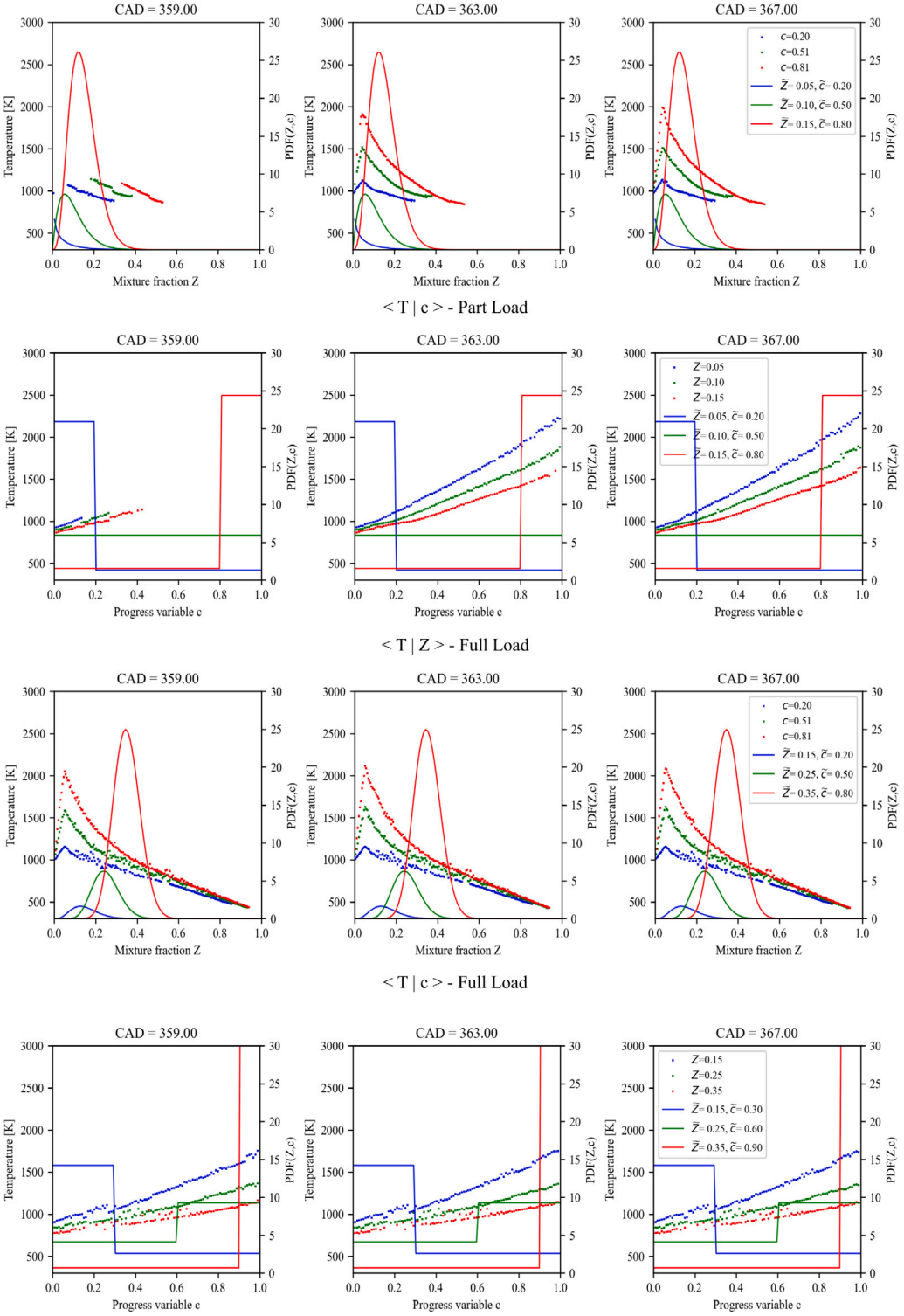

Fig. 9. Representation of the joint probability density function for Z and c and their overlap with the LEM solution in Z and c spaces, respectively. Part Load (above) and Full Load (below) at CAD = 359.00 (left), 363.00 (center), 367.00 (right). All β-PDFs are constructed with a variance of 0.004. (For interpretation of the references to color in this figure legend, the reader is referred to the web version of this article.)

with non-vanishing PDF values and available LEM solution data can be observed from the plots in Fig. 9. This is, however, only achievable with utilization of multiple LEMs.

4.4. LEM solution scatter plots

Fig. 8 shows MRILEM scatter plots of temperature, CO and OH mass fractions at CAD = 367 conditioned on mixture fraction for the part-load and the full-load case. The individual solution points correspond to the occupation of (Z, c)-space as depicted in Fig. 7. For example, from the CO mass fraction plots, a zone with no values exists at CAD = 367 for part load and fuel-rich mixtures with $Z > 0.35$. This gap can be comprehended when examining Figs. 7 and 8; CO is an intermediate specie so it will have values only in regions in the middle of c space. However, when looking at Fig. 7 CAD = 367 part-load, MRILEM does not have values of c for $Z > 0.35$ due to LEM fuel injection and turbulent advection, which explains the gap that appears

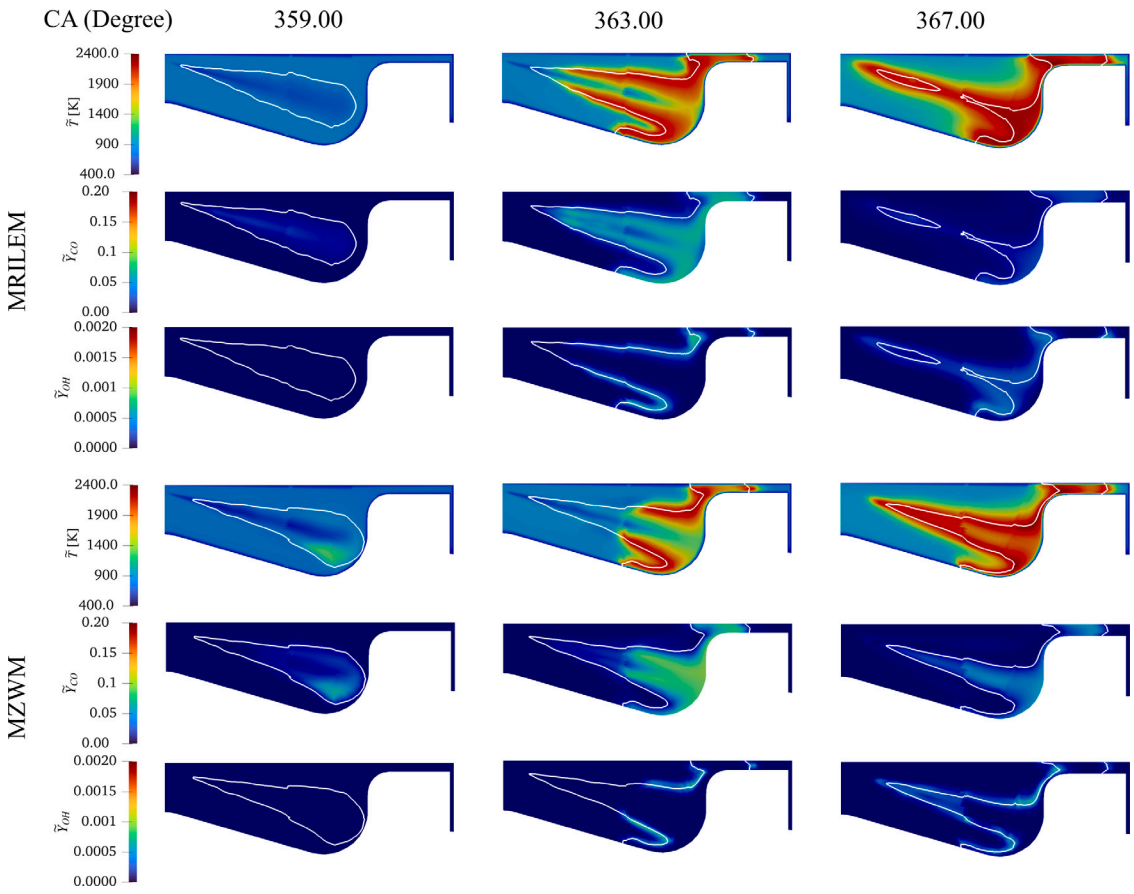

Fig. 10. CFD results of MRILEM and MZWM for the part-load case for CAD = 359.00, 363.00, 367.00.

in Fig. 7. Higher peak temperatures and CO mass fractions are observed for the full-load case compared to the part-load case due to the higher amount of injected fuel leading to higher pressure. However, the scatter plots for OH mass fraction are very similar for both load cases.

4.5. CFD results

Figs. 10 and 11 show the development of the flame structure and intermediate species CO and OH mass fraction distribution for the MZWM and MRILEM model, respectively. The plots summarize simulation results for three crank angle degrees for both part- and full-load conditions. It is well known that turbulence-chemistry interaction (TCI) is very important in turbulent combustion and that in particular pollutant formation is sensitive to TCI [49,50]. Therefore it is interesting to compare MZWM and MRILEM as the former model does not address TCI explicitly whereas MRILEM (or LEM to start with) does. The white iso-lines in the figure plots mark stoichiometric mixture conditions $Z_{st} = 0.045$ for part-load and $Z_{st} = 0.049$ for full-load. Overall the solutions computed from both models are quite similar with some relevant differences discussed below. The small discontinuities seen in the middle of the computational domain are an artifact of the mesh and have been observed in previous studies using the same mesh before [31].

Part-load case

CAD = 359 corresponds to the start of the injection. An increase in temperature and CO mass fraction indicating the start of combustion can be noticed in the MZWM close to the wall. However, OH mass fraction values are still insignificant. No indication for start of combustion is observed for MRILEM yet. This is consistent with Fig. 7 at CAD = 359 for part-load where no solution is available for high progress variable values at Z_{st}. The stoichiometric mixture fraction surface has developed slightly differently for the two models. It reaches the piston wall earlier in the MZWM model than in MRILEM. This is due to a slightly earlier ignition in the MZWM model with higher temperatures at earlier CAD values which promote fuel evaporation compared to MRILEM.

Ignition in MRILEM will always start on the LEM side first and communicated to the CFD side via the reaction progress variable source term $\dot{c}$, i.e., combustion progress on the CFD side will be retarded relative to the LEM side by at least one-time step. This is to be expected in a fractional time stepping scheme with operator splitting and hardly noticeable due to the very small time steps typically used for stability reasons in engine simulations.

At CAD = 363, the white iso-contours display a similar shape for the two models and both models show strong combustion going on. The temperature field, however, appears to have developed differently. The MZWM features a more compact flame close to the cylinder wall, whereas in MRILEM, the flame extends further towards the injector nozzle along stoichiometric mixture. This might be interpreted as an effect of TCI which, in this case, enhances combustion. Similar trends are observed for CO and OH mass fractions. Fig. 7 shows for this CAD value a fully occupied c-space for $Z = Z_{st}$ confirming both strong combustion and still unreacted fuel–air mixture at $c = 0$.

At CAD = 367, the extend of the high-temperature region has moved further upstream along the cone of stoichiometric mixture for the MZWM and even more for MRILEM. Furthermore, the lines of stoichiometric mixture have collapsed already in some parts along the spray axis for MRILEM indicating a combustion progress ahead of the MZWM where the isolines of stoichiometric mixture forming a cone are still well separated. The observed results together with the retarded ignition in MRILEM compared to MZWM clearly indicate an overall shorter combustion period in MRILEM which can be explained by strong TCI interaction in MRILEM enhancing combustion. Higher

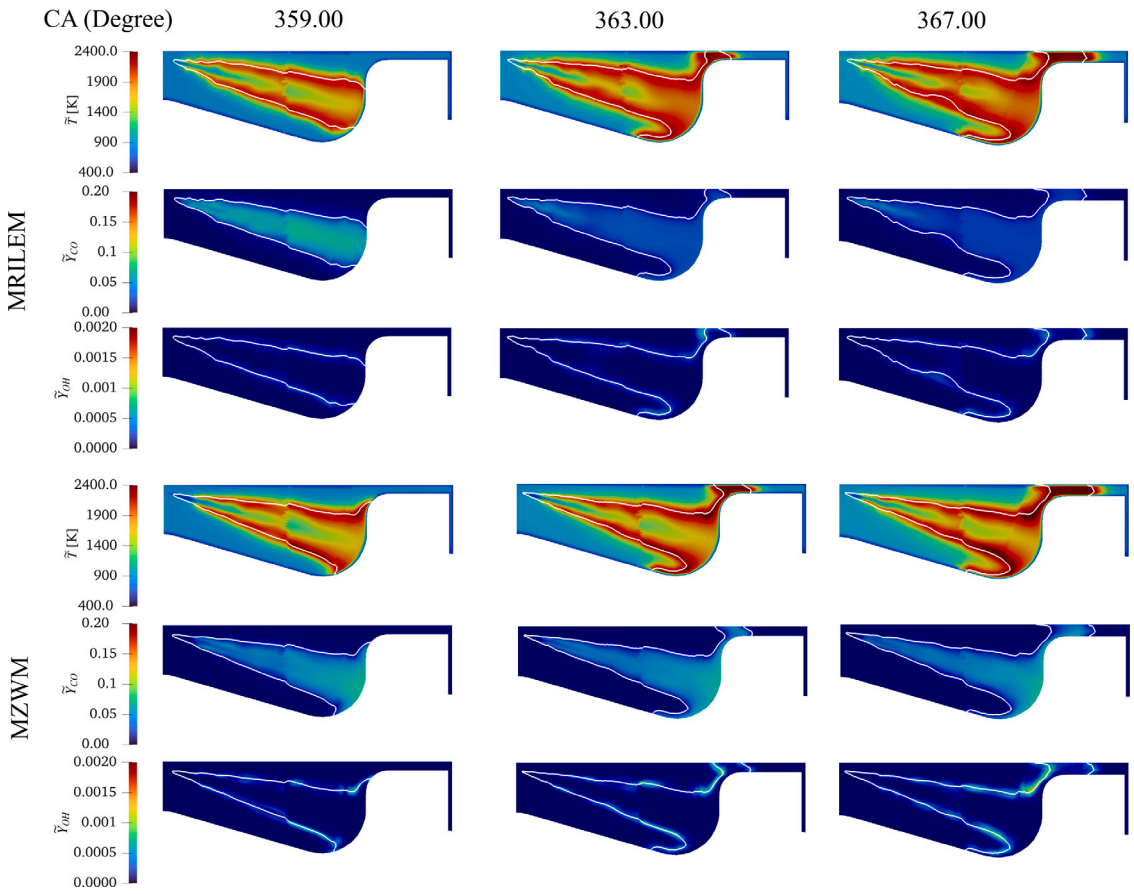

Fig. 11. CFD results of MRILEM and MZWM for the full-load case for CAD = 359.00, 363.00, 367.00.

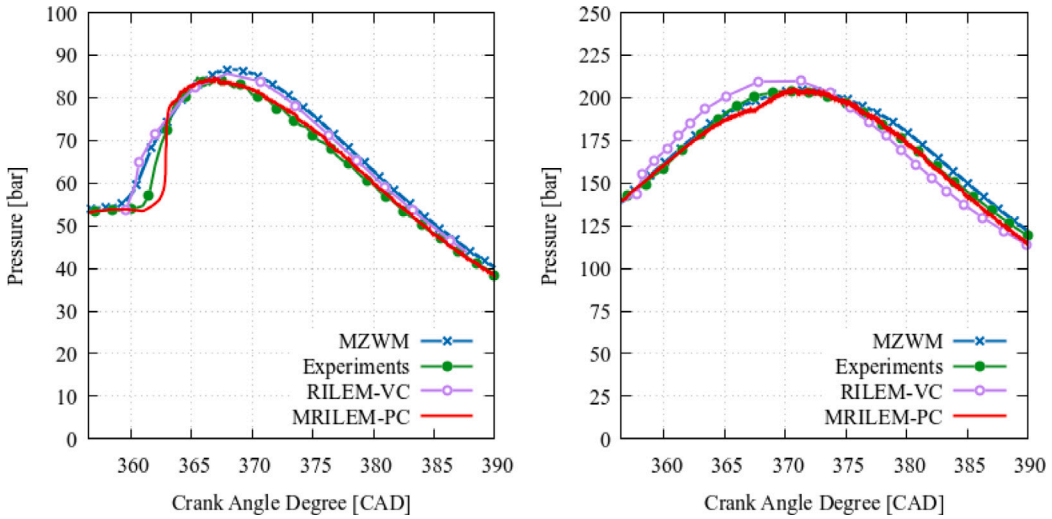

Fig. 12. Comparison of pressure trace between MRILEM-PC, RILEM-VC, MZWM and experiments for the part-load (left) and full-load (right) cases.

peak temperatures close to the nozzle are observed for MRILEM at this CAD.

Full-Load

Contrary to the part-load case, the solution table at CAD = 359 for the full-load appearing in Fig. 7 is almost completely for the relevant regions in (Z, c)-space. At full-load, injection starts earlier compared to part-load leaving more time for fuel-air mixing. In addition, higher pressure values and overall more fuel lead to stronger and faster and combustion. A complete filled solution space prevents any potential artifacts steaming from PDF scaling as described in Section 2.5 which affects mass fraction values and temperature.

Similarly to the part-load case, the stoichiometric mixture fraction isoline has clearly advanced further at CAD = 359 in the MZWM model compared to MRILEM. In MRILEM the tip of the flame is just hitting the wall which has occurred earlier in the MZWM model. However, the elongation of the flame up to the injector is comparable for both model. At CAD = 363 the shape of the stoichiometric mixture fraction isolines look very similar for both models, which implies that combustion between CAD = 359 and 363 was faster in the RILEM

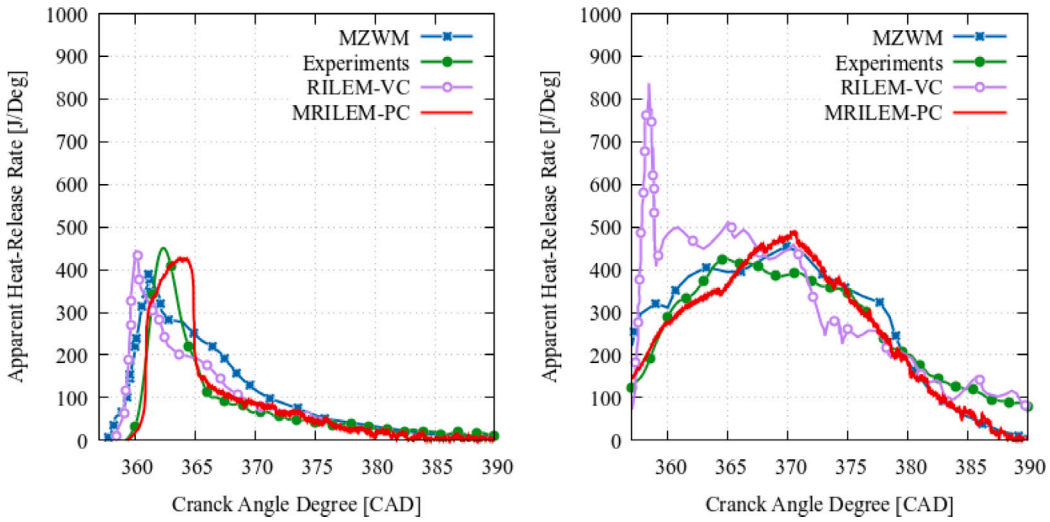

Fig. 13. Comparison of heat release rate between MRILEM-PC, RILEM-VC, MZWM and experiments for the part-load (left) and full-load (right) cases.

case than in the MZWM model. However, substantial differences can be observed for CO mass fractions at CAD = 363: within the fuel-rich area inside the cone of the stoichiometric mixture the RILEM shows substantially lower values compared to the MZWM model. These high CO levels are maintained in the MZWM model advancing from CAD = 363 to CAD = 367. MRILEM maintains its CO level as well with a small decrease. The differences between the MZWM model and MRILEM are less pronounced for OH. Both models create high OH mass fraction values around the stoichiometric mixture, but the zone with high OH values appears wider for the MZWM model indicating a broader reaction zone compared to MRILEM. This is likely due to the full spatial resolution of flame structures on the LEM, which allow the representation of sharp reaction fronts smeared in the MZWM model.

4.6. Pressure traces

Pressure traces extracted from volume-coupled RILEM with one LEM line (RILEM-VC), pressure-coupled MRILEM-PC, MZWM, and experiments for part- and full-load are displayed in Fig. 12. The MRILEM-PC pressure trace for part-load yields good agreement with the experimental results. Ignition for MZWM and RILEM-VC happens simultaneously and earlier than in the experiment. MRILEM-PC, on the other hand, ignites slightly later. However, the tail of the pressure trace is much better represented by MRILEM-PC than by MZWM or RILEM-VC for part load. MRILEM-PC and MZWM both capture the full-load pressure trace well. Additionally, MRILEM-PC outperforms RILEM-VC, which overpredicts the full-load pressure trace until CAD = 372 and then underpredicts it for the rest of cycle. MRILEM-PC also manages to predict the tail of the pressure trace better than MZWM and RILEM-VC.

4.7. Apparent heat-release rate (AHRR)

Fig. 13 shows results of the AHRR for volume-coupled RILEM with one LEM line (RILEM-VC), pressure-coupled MRILEM-PC, MZWM, and experiments for both the part- and full-load cases. MRILEM-PC provides good agreement for the part-load case's initial stages of the AHRR curve. The MZWM and RILEM-VC predict a too early ignition compared with the experiment for part-load, as observed in 12. MRILEM-PC, RILEM-VC, and MZWM predict a similar heat release peak value for the part-load case; however, slightly less than the experimental result. The heat release peak for MRILEM-PC happens late in the part-load case compared to the experiments, likely due to a shortage of representative LEM data at that simulation stage. The AHRR tail is well predicted by MRILEM-PC and RILEM-VC in the part-load case and slightly over-predicted by the MZWM. MRILEM-PC also delivers a good agreement on the full-load case at the initial phases of the curve. A high peak of heat release can be observed for RILEM-VC full-load, which is also reflected by the pressure mismatch in Fig. 12. This most likely occurs due to missing LEM solutions in (Z, c)-space advancing just one LEM line. MZWM ignition prediction is better than RILEM-VC, but MRILEM-PC reveals the best ignition prediction for the full-load case. MRILEM-PC over-predicts the heat release peak by a similar proportion as the MZWM. MRILEM-PC underpredicts the AHRR tail, as does the MZWM. However, RILEM-VC captures the tail of the heat release curve relatively better than MRILEM-PC and MZWM. It is important to note that the MZWM model was tuned to match the pressure trace on the experiments, which was not the case for MRILEM-PC or RILEM-VC. A reason for the better agreement of MRILEM-PC compared to MZWM could be the proper consideration of turbulence chemistry interaction (TCI) on the individual LEM lines in MRILEM-PC, whereas no TCI is considered in the MZWM model. However, the inclusion of TCI in RILEM is not the only reason behind the superior performance of MRILEM-PC since RILEM-VC also includes TCI effects. In addition, MRILEM-PC advances multiple LEM lines, providing a more statistically more sound solution than a single LEM in RILEM-VC and captures heat loss effects due to the pressure coupling in a more consistent way.

5. Conclusion

This paper presents substantial developments of the recently presented Representative Interactive Linear Eddy Model (RILEM) [26,31] to simulate turbulent non-premixed combustion in internal combustion engines. The main purpose of this work was to improve the statistical fidelity of the model. RILEM utilizes the Linear Eddy Model and a presumed PDF approach for combustion closure. In particular, the following developments have been discussed:

- Introduction of a pressure based coupling between the LEM combustion model and the CFD flow solver,
- Introduction of a presumed PDF for the reaction progress variable,
- Consideration of multiple LEMs (MRILEM).

Compared to the volume based coupling in the original RILEM version [26], the pressure based coupling features an intrinsic communication of heat losses, e.g wall heat losses and latent heat of evaporation, from the CFD flow solver to the LEM model. These required explicit modeling in the volume based coupling approach. In the pressure based coupling the spatially constant pressures on the CFD domain and the LEM match which leads to a weak coupling among individual LEMs in MRILEM. The introduction of a reaction progress

variable for RILEM in [31] with a delta-peak PDF was further refined by consideration of more realistic PDF shapes. MRILEM was particularly developed to address the issue of an incomplete solution space in mixture fraction and progress variable space on a single LEM which is required to perform calculations of mean values via integration of scalar values with the (presumed) PDF. Running multiple LEM lines with different turbulence statistics was an essential step to increase the density of the solution table and increases the statistical fidelity of the simulation approach.

Good agreement was observed for the pressure based MRILEM for both the part- and full-load cases, when compared to simulations with a multi-zone well-mixed (MZWM) model and experimental pressure traces. The effects of including turbulent chemistry interactions were observed in the solution table representation and in the CFD results, namely in the flame structure and CO concentrations when comparing MRILEM and MZWM. It is important to note that the results reached with MRILEM were not subject to any tuning. The fidelity of MRILEM can potentially be further improved by increasing the number of LEM lines and by tuning some key CFD parameters such as vapor and liquid penetration length which were not available for the investigated testcases.

RILEM is a strong candidate to simulate challenging engine configurations such as dual fuel combustion, mixed mode combustion or consideration of differential diffusion effects in hydrogen combustion as the direct resolution of all microphysical phenomena on the LEM line allows a straightforward implementation of such configurations.

CRediT authorship contribution statement

Nidal Doubiani: Conceptualization, Methodology, Programming, Simulations, Investigation, Writing – original draft, Visualization. **Alan R. Kerstein:** Conceptualization, Methodology, Investigation, Supervision, Writing – review & editing. **Michael Oevermann:** Conceptualization, Methodology, Investigation, Resources, Writing – review & editing, Supervision, Project administration, Funding acquisition.

Declaration of competing interest

The authors declare that they have no known competing financial interests or personal relationships that could have appeared to influence the work reported in this paper.

Data availability

Data will be made available on request.

Acknowledgments

The authors thank Chalmers Combustion Engine Research Center (CERC) for their financial support and acknowledge the Swedish National Infrastructure for Computing (SNIC) at the Chalmers Centre for Computational Science and Engineering (C3SE) for providing the compute and storage resources needed for this work via projects SNIC 2022/1-9, SNIC 2022/23-605 and SNIC 2021/23-640.

References

[1] Ritchie H. Cars, planes, trains: where do CO2 emissions from transport come from, vol. 6. Our World in Data; 2020.
[2] Peters N. Laminar flamelet concepts in turbulent combustion. Symp (Int) Combust 1988;21(1):1231–50. http://dx.doi.org/10.1016/S0082-0784(88)80355-2.
[3] Pitsch H, Peters N. A consistent flamelet formulation for non-premixed combustion considering differential diffusion effects. Combust Flame 1998;114(1):26–40. http://dx.doi.org/10.1016/S0010-2180(97)00278-2.
[4] Benim AC, Syed KJ. Laminar flamelet modelling of turbulent premixed combustion. Appl Math Model 1998;22(1):113–36. http://dx.doi.org/10.1016/S0307-904X(98)00012-2.
[5] Nilsson P, Bai XS. Level-set flamelet library approach for premixed turbulent combustion. Exp Therm Fluid Sci 2000;21(1):87–98. http://dx.doi.org/10.1016/S0894-1777(99)00058-8.
[6] Maghbouli A, Lucchini T, D'Errico G, Onorati A, Malbec L-M, Musculus MP, Eagle WE. Parametric comparison of well-mixed and flamelet n-dodecane spray combustion with engine experiments at well controlled boundary conditions. Tech. rep, SAE Technical Paper; 2016.
[7] Pei Y, Hawkes ER, Kook S. A comprehensive study of effects of mixing and chemical kinetic models on predictions of n-heptane jet ignitions with the PDF method. Flow Turbul Combust 2013;91(2):249–80. http://dx.doi.org/10.1007/s10494-013-9454-z.
[8] Pope S. PDF methods for turbulent reactive flows. Prog Energy Combust Sci 1985;11(2):119–92. http://dx.doi.org/10.1016/0360-1285(85)90002-4.
[9] Bolla M, Chishty MA, Hawkes ER, Kook S. Modeling combustion under engine combustion network Spray A conditions with multiple injections using the transported probability density function method. Int J Engine Res 2017;18(1–2):6–14. http://dx.doi.org/10.1177/1468087416689174.
[10] Xu S, Pang KM, Li Y, Hadadpour A, Yu S, Zhong S, Jangi M, Bai X-s. LES/TPDF investigation of the effects of ambient methanol concentration on pilot fuel ignition characteristics and reaction front structures. Fuel 2021;287:119502. http://dx.doi.org/10.1016/j.fuel.2020.119502.
[11] Zhao M, Chen ZX, Zhang H, Swaminathan N. Large eddy simulation of a supersonic lifted hydrogen flame with perfectly stirred reactor model. Combust Flame 2021;230:111441. http://dx.doi.org/10.1016/j.combustflame.2021.111441.
[12] Lu H, Zou C, Shao S, Yao H. Large-eddy simulation of MILD combustion using partially stirred reactor approach. Proc Combust Inst 2019;37(4):4507–18. http://dx.doi.org/10.1016/j.proci.2018.09.032.
[13] Petrova N, Sabelnikov V, Bertier N. Numerical simulation of a backward-facing step combustor using reynolds-averaged navier–stokes / extended partially stirred reactor model. In: Progress in propulsion physics – volume 11. Krakow, Poland: EDP Sciences; 2019, p. 625–56. http://dx.doi.org/10.1051/eucass/201911625.
[14] Kerstein AR. A Linear- Eddy model of turbulent scalar transport and mixing. Combust Sci Technol 1988;60(4–6):391–421. http://dx.doi.org/10.1080/00102208808923995.
[15] Kerstein AR. Linear-eddy modeling of turbulent transport. II: Application to shear layer mixing. Combust Flame 1989;75(3):397–413. http://dx.doi.org/10.1016/0010-2180(89)90051-5.
[16] Kerstein AR. Linear-eddy modelling of turbulent transport. Part 3. Mixing and differential molecular diffusion in round jets. J Fluid Mech 1990;216:411–35. http://dx.doi.org/10.1017/S0022112090000489, Publisher: Cambridge University Press.
[17] Kerstein AR. Linear-eddy modelling of turbulent transport. Part 6. Microstructure of diffusive scalar mixing fields. J Fluid Mech 1991;231:361–94. http://dx.doi.org/10.1017/S0022112091003439.
[18] Kerstein AR. Linear-eddy modelling of turbulent transport. Part 7. Finite-rate chemistry and multi-stream mixing. J Fluid Mech 1992;240:289–313. http://dx.doi.org/10.1017/S0022112092000107, Publisher: Cambridge University Press.
[19] McMurtry P, Menon S, Kerstein A. Linear eddy modeling of turbulent combustion. Energy Fuels 1993;7(6):817–26. http://dx.doi.org/10.1021/ef00042a018.
[20] Menon S, Calhoon WH. Subgrid mixing and molecular transport modeling in a reacting shear layer. Symp (Int) Combust 1996;26(1):59–66. http://dx.doi.org/10.1016/S0082-0784(96)80200-1.
[21] Arshad S. Large eddy simulation of combustion using linear-eddy subgrid modeling. no. ny serie nr. 4563 in Doktorsavhandlingar vid chalmers tekniska högskola, Göteborg, Sweden: Chalmers University of Technology; 2019.
[22] McMurthy PA, Menon S, Kerstein AR. A linear eddy sub-grid model for turbulent reacting flows: Application to hydrogen-air combustion. Symp (Int) Combust 1992;24(1):271–8. http://dx.doi.org/10.1016/S0082-0784(06)80036-6.
[23] Arshad S, Kong B, Kerstein A, Oevermann M. A strategy for large-scale scalar advection in large eddy simulations that use the linear eddy sub-grid mixing model. Internat J Numer Methods Heat Fluid Flow 2018;28(10):2463–79. http://dx.doi.org/10.1108/HFF-09-2017-0387.
[24] Chakravarthy V, Menon S. Subgrid modeling of turbulent premixed flames in the flamelet regime. Flow Turbul Combust 2000;65(2):133–61. http://dx.doi.org/10.1023/A:1011456218761.
[25] Arshad S, Gonzalez-Juez E, Dasgupta A, Menon S, Oevermann M. Subgrid reaction-diffusion closure for large eddy simulations using the linear-eddy model. Flow Turbul Combust 2019;103:389–416. http://dx.doi.org/10.1007/s10494-019-00019-x.
[26] Lackmann T, Kerstein AR, Oevermann M. A representative linear eddy model for simulating spray combustion in engines (RILEM). Combust Flame 2018;193:1–15. http://dx.doi.org/10.1016/j.combustflame.2018.02.008.
[27] Barths H, Antoni C, Peters N. Three-dimensional simulation of pollutant formation in a DI diesel engine using multiple interactive flamelets. SAE technical paper 982459, Warrendale, PA: SAE International; 1998, http://dx.doi.org/10.4271/982459, iSSN: 0148-7191, 2688-3627.
[28] D'Errico G, Lucchini T, Contino F, Jangi M, Bai X-S. Comparison of well-mixed and multiple representative interactive flamelet approaches for diesel spray combustion modelling. Combust Theory Model 2014;18(1):65–88. http://dx.doi.org/10.1080/13647830.2013.860238.

[29] Gao Z, Jiang C, Lee C-H. Representative interactive flamelet model and flamelet/progress variable model for supersonic combustion flows. Proc Combust Inst 2017;36(2):2937–46. http://dx.doi.org/10.1016/j.proci.2016.06.184.
[30] Lackmann T, Lucchini T, D'Errico G, Kerstein A, Oevermann M. Modeling n-dodecane spray combustion with a representative interactive linear eddy model. SAE technical papers 2017-March (March), 2017, http://dx.doi.org/10.4271/2017-01-0571.
[31] Lackmann T, Nygren A, Karlsson A, Oevermann M. Investigation of turbulence–chemistry interactions in a heavy-duty diesel engine with a representative interactive linear eddy model. Int J Engine Res 2020;21(8):1469–79. http://dx.doi.org/10.1177/1468087418812319, Publisher: SAGE Publications.
[32] Doubiani N, Menon A, Kerstein AR, Oevermann M. Pressure coupling of the spherical linear eddy model to RANS-CFD for internal-combustion engine simulation. In: Proceedings of the 6th world congress on momentum, heat and mass transfer (MHMT'21). 2021, 103–1–103–8. http://dx.doi.org/10.11159/csp21.lx.103.
[33] Jochim B, Korkmaz M, Pitsch H. Scalar dissipation rate based multi-zone model for early-injected and conventional diesel engine combustion. Combust Flame 2017;175:138–54. http://dx.doi.org/10.1016/j.combustflame.2016.08.003.
[34] Smith TM, Menon S. One-dimensional simulations of freely propagating turbulent premixed flames. Combust Sci Technol 1997;128(1–6):99–130. http://dx.doi.org/10.1080/00102209708935706.
[35] Hindmarsh AC, Brown PN, Grant KE, Lee SL, Serban R, Shumaker DE, Woodward CS. SUNDIALS: Suite of nonlinear and differential/algebraic equation solvers. ACM Trans Math Softw 2005;31(3):363–96. http://dx.doi.org/10.1145/1089014.1089020.
[36] Bhattacharjee S, Haworth DC. Simulations of transient n-heptane and n-dodecane spray flames under engine-relevant conditions using a transported PDF method. Combust Flame 2013;160(10):2083–102. http://dx.doi.org/10.1016/j.combustflame.2013.05.003.
[37] Pierce CD, Moin P. Progress-variable approach for large-eddy simulation of non-premixed turbulent combustion. J Fluid Mech 2004;504:73–97. http://dx.doi.org/10.1017/S0022112004008213.
[38] Goodwin DG. Cantera: An object-oriented software toolkit for chemical kinetics, thermodynamics, and transport processes. Tech. rep, Pasadena: Caltech; 2009.
[39] Lucchini T, D'Errico G, Brusiani F, Bianchi GM. MS2-3: A finite-element based mesh motion technique for internal combustion engine simulations(MS: Modeling and simulation,general session papers). In: The international symposium on diagnostics and modeling of combustion in internal combustion engines 2008.7. 2008, p. 671–8. http://dx.doi.org/10.1299/jmsesdm.2008.7.671.
[40] Huh K, Gosman A. A phenomenological model of diesel spray atomization. In: Proceedings of the international conference on multiphase flows. Tsukuba, Japan; 1991.
[41] Pilch M, Erdman CA. Use of breakup time data and velocity history data to predict the maximum size of stable fragments for acceleration-induced breakup of a liquid drop. Int J Multiph Flow 1987;13(6):741–57. http://dx.doi.org/10.1016/0301-9322(87)90063-2.
[42] Ranz WE, Marshall WM. Evaporation from drops, Parts I & II. Chem Eng Prog 1952;48:141–6.
[43] Maghbouli A, Lucchini T, D'Errico G, Onorati A. Effects of grid alignment on modeling the spray and mixing process in direct injection diesel engines under non-reacting operating conditions. Appl Therm Eng 2015;91:901–12. http://dx.doi.org/10.1016/j.applthermaleng.2015.07.051.
[44] Aceves SM, Flowers DL, Westbrook CK, Smith JR, Pitz W, Dibble R, Christensen M, Johansson B. A multi-zone model for prediction of HCCI combustion and emissions. SAE Trans 2000;431–41. http://dx.doi.org/10.4271/2000-01-0327.
[45] Weller HG, Tabor G, Jasak H, Fureby C. A tensorial approach to computational continuum mechanics using object-oriented techniques. Comput Phys 1998;12(6):620–31. http://dx.doi.org/10.1063/1.168744, Publisher: American Institute of Physics.
[46] Lignell DO, Lansinger VB, Medina J, Klein M, Kerstein AR, Schmidt H, Fistler M, Oevermann M. One-dimensional turbulence modeling for cylindrical and spherical flows: model formulation and application. Theor Comput Fluid Dyn 2018;32(4):495–520. http://dx.doi.org/10.1007/s00162-018-0465-1.
[47] Lucchini T, Torre AD, D'Errico G, Montenegro G, Fiocco M, Maghbouli A. Automatic mesh generation for CFD simulations of direct-injection engines. SAE technical paper 2015-01-0376, Warrendale, PA: SAE International; 2015, http://dx.doi.org/10.4271/2015-01-0376, iSSN: 0148-7191, 2688-3627.
[48] Yao T, Pei Y, Zhong B, Som S. A hybrid mechanism for n-dodecane combustion with optimized low-temperature chemistry. In: Proceedings of the 9th US national combustion meeting. Cincinnati, OH; 2015, p. 1141C–0055.
[49] Borghesi G, Mastorakos E, Devaud CB, Bilger RW. Modeling evaporation effects in conditional moment closure for spray autoignition. Combust Theory Model 2011;15(5):725–52. http://dx.doi.org/10.1080/13647830.2011.560282.
[50] Pei Y, Hawkes ER, Kook S. Transported probability density function modelling of the vapour phase of an n-heptane jet at diesel engine conditions. Proc Combust Inst 2013;34(2):3039–47. http://dx.doi.org/10.1016/j.proci.2012.07.033.